Composition Space Diagrams for Mixed Transition Metal Oxide Fluorides

Alexander J. Norquist, Kevin R. Heier, Charlotte L. Stern, and Kenneth R. Poeppelmeier*

Department of Chemistry, Northwestern University, Evanston, Illinois 60208-3113

Received June 24, 1998

Composition space diagrams have been used to study phase stability of mixed transition metal oxide fluorides synthesized by hydrothermal reaction of the metal oxides in $(HF)_x$·pyridine/H_2O/pyridine solution (150 °C, autogenous pressure). The combination of early (Ti, Zr, Hf, Nb, Ta, Mo, W) and late (Cu, Cd, Zn) transition metals and the effects of varying the mole ratios of the metals, $(HF)_x$·pyridine, and water are examined in this study. Single-crystal products containing $[Cu(py)_4]^{2+}$, $[Cd(py)_4]^{2+}$, or $[Zn(py)_4]^{2+}$ cations and $[TiF_6]^{2-}$, $[ZrF_6]^{2-}$, $[HfF_6]^{2-}$, $[NbOF_5]^{2-}$, $[TaOF_5]^{2-}$, $[MoO_2F_4]^{2-}$, or $[WO_2F_4]^{2-}$ anions are recovered. Relative stability of the crystalline products is governed by the negative charge distribution on the anions, as well as the concentrations of each reactant in solution. Two new structures are reported: $Cu(NC_5H_5)_4TaOF_5$ and $Cu(NC_5H_5)_4TiF_6$·$3H_2O$. Crystal data: for $Cu(NC_5H_5)_4TaOF_5$, monoclinic, space group *C2/c* (No. 15), with $a = 10.541(3)$ Å, $b = 13.547(6)$ Å, $c = 16.04(1)$ Å, $\beta = 97.73(5)°$, and $Z = 4$; for $Cu(NC_5H_5)_4TiF_6$·$3H_2O$, monoclinic, space group *C2/c* (No. 15), with $a = 12.767(4)$ Å, $b = 12.048(2)$ Å, $c = 17.787(6)$ Å, $\beta = 109.9(1)°$, and $Z = 4$.

Introduction

Hydrothermal reactions provide a convenient and efficient method to study the crystallization fields of mixed transition metal oxide flourides. Hydrogen fluoride is used to dissolve metal oxides under hydrothermal conditions (150 °C, autogenous pressure) in pyridinium poly(hydrogen fluoride)/H_2O/pyridine solutions. Slowly cooling these solutions results in single crystals of new mixed metal oxide fluoride compounds. In each system an early (Ti, Zr, Hf, Nb, Ta, Mo, W) and a late (Cu, Cd, Zn) transition metal are used. The early transition metals are "hard" acids and coordinate the "hard" bases in solution (F^- and O^{2-}), while the late transition metals are "soft" acids and coordinate the "soft" bases in solution (pyridine (py)). The "soft" metals form $[Cu(py)_4]^{2+}$, $[Cd(py)_4]^{2+}$, and $[Zn(py)_4]^{2+}$ cations, while the "hard" metals form $[TiF_6]^{2-}$, $[ZrF_6]^{2-}$, $[HfF_6]^{2-}$, $[NbOF_5]^{2-}$, $[TaOF_5]^{2-}$, $[MoO_2F_4]^{2-}$, and $[WO_2F_4]^{2-}$ anions. Other important species, such as hydronium (H_3O^+) and pyridinium (pyH^+) cations and F^- anions, are also present in solution. Which species combine to form the crystalline products depends on the negative charge distribution on the anions, the fluoride affinity of the cations, and the mole fraction in solution of each reaction component (Figure 1).

To report the variables involved in these hydrothermal reactions, "composition space" diagrams have been developed. Composition space diagrams are similar to ternary phase diagrams in that the products are directly related to initial reactant mole fractions. The concentration of the three reactants, namely, metal oxides, $(HF)_x$·pyridine, and H_2O, are recorded in each composition space diagram. Approximately 20 reactions are run at varying mole fractions of each of these reactants, while other variables such as temperature and amount of solvent are held constant.[1] The crystalline products of the reactions are analyzed and the results plotted on the diagram to determine "crystallization fields", that is, areas of selective crystallization, for each product. Composition space diagrams are not phase diagrams as only the crystalline products are analyzed, while products which are amorphous or remain in solution are neglected. In addition, the boundaries separating the crystallization fields are not sharp. In the area adjacent to a boundary, a mixture of crystalline products is often observed. Nevertheless, the composition space diagram is a useful tool to help plan reactions and rationalize the results in hydrothermal systems.

Composition space diagrams have been reported previously for the (MO_x, $^1/_2Nb_2O_5$)/$(HF)_x$·pyridine/H_2O (MO_x = CuO,[1] CdO[2]) systems. Composition space diagrams for the (CuO, $M'O_x$)/$(HF)_x$·pyridine/H_2O ($M'O_x$ = TiO_2, ZrO_2, HfO_2, $^1/_2Ta_2O_5$, MoO_3, WO_3) and (ZnO, $^1/_2Nb_2O_5$)/$(HF)_x$·pyridine/H_2O systems are reported here. Composition space diagrams for the (CuO, xWO_3)/$(HF)_x$·pyridine/H_2O (x = 0.5, 1, 2) series are also reported. The structures for two new mixed metal oxide fluoride compounds, $Cu(py)_4TaOF_5$ and $Cu(py)_4TiF_6$·$3H_2O$ (py = pyridine), are reported in the Supporting Information.

Experimental Section

CAUTION! $(HF)_x$·pyridine is toxic and corrosive.

Materials. CuO (99%, Aldrich), MoO_3 (99.5%, Aldrich), ZrO_2 (99%, Aldrich), TiO_2 (99.9%, Aldrich), Nb_2O_5 (99.99%, Aldrich), WO_3 (99%, Aldrich), CdO (99.5%, Aldrich), Ta_2O_5 (99.99%, Aldrich), HfO_2 (98%, Aldrich), ZnO (99%, Aldrich), pyridine (99.8%, anhydrous, Aldrich), and $(HF)_x$·pyridine (pyridinium poly(hydrogen fluoride), 70 wt % HF, Aldrich) were used as received. Reagent amounts of deionized H_2O were used in the syntheses.

* Corresponding author.

(1) Halasyamani, P.; Willis, M. J.; Stern, C. L.; Lundquist, P. M.; Wong, G. K.; Poeppelmeier, K. R. *Inorg. Chem.* **1996**, *35*, 1367.
(2) Halasyamani, P. S.; Heier, K. R.; Norquist, A. J.; Stern, C. L.; Poeppelmeier, K. R. *Inorg. Chem.* **1998,** *37*, 369.

10.1021/ic9807238 CCC: $15.00
Published on Web 11/20/1998

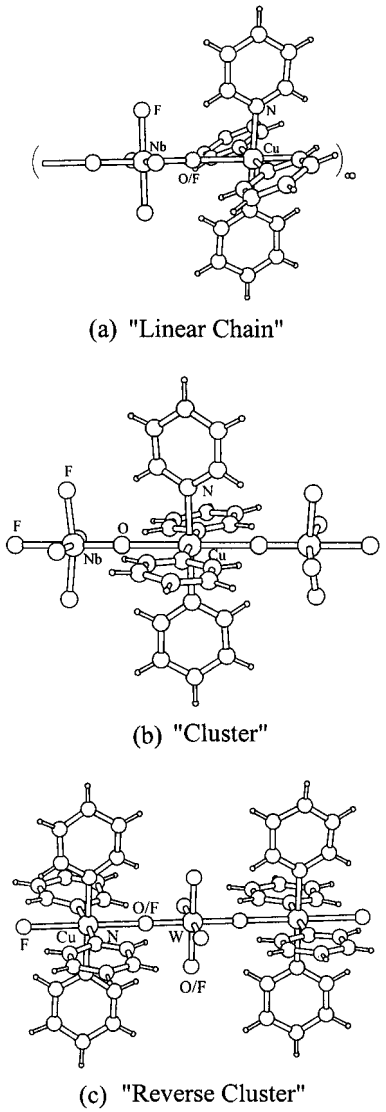

Figure 1. Examples of the three main structure types: (a) "linear chain" compound ($Cu(py)_4NbOF_5$), (b) "cluster" compound ($[pyH]_2[Cu(py)_4(NbOF_5)_2]$), and (c) "reverse cluster" compound ($[(CuF(py)_4)_2WO_2F_4][H_3O]_2[F]_2$).

Synthesis. All composition space diagrams were constructed in a similar manner. Individual reaction points for each composition space diagram are available in the Supporting Information. Appropriate amounts of metal oxides, $(HF)_x$·pyridine, and H_2O reactants were placed along with 1.5 g (1.26×10^{-2} mol) of solvent pyridine in a Teflon (fluoro(ethylene-propylene)) "pouch".[3] Mole fractions of the reactants were varied, with the total number of moles held constant (7.5×10^{-3} mol). The pouches were sealed and placed into a 2000-mL autoclave (Parr) filled with 600 mL of deionized water. Several reactions with different mole fractions of each reactant were placed in the autoclave at the same time, ensuring that all reactions took place at the same temperature and pressure. The autoclave was sealed and heated at 150 °C for 24 h and then slow cooled to room temperature over an additional 24 h. In some cases, faster cooling resulted in polycrystalline material or smaller crystals. After reaction, each pouch contained both solid products and solution. To recover the solid, the pouches were opened in air and recovered by filtration, usually in 30−70% yield based on early transition metal. The crystalline products were analyzed by powder XRD and single-crystal XRD. Crystallization fields became evident as different compounds crystallized in different regions of the composition space (see Figures 2−4).

Crystallographic Determination. Relevant crystallographic data for $Cu(py)_4TaOF_5$ and $Cu(py)_4TiF_6·3H_2O$ are listed in Table 1. Atomic coordinates, isotropic thermal parameters, and principal bond distances and angles are available in the Supporting Information. All data was collected on a CAD4 diffractometer. All calculations were performed using the TEXSAN crystallographic software package from Molecular Structure Corporation.[4] The structures were solved by direct methods[5] and expanded using Fourier techniques.[6]

Crystal Structure of $Cu(py)_4TaOF_5$. On the basis of systematic absences and successful solution and refinement of the structure, the space group was determined to be *C2/c* (No. 15). Disorder in the acentric $[TaOF_5]^{2-}$ anion resulted in Ta occupying an inversion center in the structure. All non-hydrogen atoms were refined anisotropically. Hydrogen atoms were placed in idealized positions. This compound is isostructural to $Cu(py)_4NbOF_5$.[1]

Crystal Structure of $Cu(py)_4TiF_6·3H_2O$. On the basis of systematic absences and successful solution and refinement of the structure, the space group was determined to be *C2/c* (No. 15). All non-hydrogen atoms were refined anisotropically. Hydrogen atoms were placed in idealized positions.

Spectroscopic Measurements. Mid-infrared (400−4000 cm^{-1}) spectra were collected using a Bio-Rad FTS-60 FTIR spectrometer operating at a resolution of 2 cm^{-1}.

Characteristic stretches were used to distinguish coordinated pyridine (1610 and 640 cm^{-1}) from pyridinium (1630, 1530, 1335, 1255 cm^{-1}).[7] Metal−oxo stretches were also identified by their infrared signatures (Nb═O, 905−890 cm^{-1}; Ta═O, 896 cm^{-1}; Mo═O, ν_s 943−938 cm^{-1}, ν_{as} 894−888 cm^{-1}; W═O, ν_s 952−943 cm^{-1}, ν_{as} 895−886 cm^{-1}).[8]

Results and Discussion

Three main structure types are observed in these systems: the "linear chain", "cluster", and "reverse cluster" structures (Figure 1). The linear chain structures, $M(py)_4M'X_6$, consist of infinite chains of alternating $[M(py)_4]^{2+}$ cations and $[M'X_6]^{2-}$ anions. The cluster structures, $[pyH]_2[M(py)_4(M'X_6)_2]$, contain discrete anions consisting of two $[M'X_6]^{2-}$ anions surrounding a central $[M(py)_4]^{2+}$ cation. Lattice pyridinium hydrogen bonds to fluoride ligands on the anion and balances the charge. Finally, the reverse cluster structures,[9] $[(CuF(py)_4)_2M'X_6][H_3O]_2[F]_2$, contain two $[CuF(py)_4]^+$ cations surrounding a central $[M'X_6]^{2-}$ anion. H_3O^+ and F^- occupy channels in the structure, creating an extensive hydrogen-bonding network. Composition space diagrams showing the crystallization fields of the structure types for each system studied are shown in Figures 2−4.

Outside the crystallization fields, each composition space diagram shows two other regions, one at high metal oxide mole fraction and one at high $(HF)_x$·pyridine mole fraction. At high metal oxide mole fractions there is not enough HF in the reaction to completely dissolve the oxides. Solid metal oxide is present throughout the reaction, providing many nucleation sites which cause the products to precipitate as very small crystallites, unsuitable for single-crystal diffraction. The reaction products in this part of the composition space are unreacted metal oxides and poorly crystalline products which were not characterized

(3) Harrison, W. T. A.; Nenoff, T. M.; Gier, T. E.; Stucky, G. D. *Inorg. Chem.* **1993**, *32*, 2437.
(4) *TEXSAN*: *Crystal Structure Analysis Package*; Molecular Structure Corp.: The Woodlands, TX, 1985 and 1992.
(5) Sheldrick, G. M. SHELXS86. In *Crystallographic Computing 3*; Sheldrick, G. M., Kruger, C., Goddard, R., Eds.; Oxford University Press: Oxford, U.K., 1985; pp 175−189.
(6) Beurskens, P. T.; Admiraal, G.; Beurskins, G.; Bosman, W. P.; de Gelder, R.; Israel, R.; Smits, J. M. M. *The DIRDIF_94 program system*; Technical Report of the Crystallography Laboratory; University of Nijmegen: Nijmegen, The Netherlands, 1994.
(7) Gill, N. S.; Nuttal, R. H.; Scaife, D. E.; Sharp, D. W. A. *Inorg. Nucl. Chem.* **1961,** *18*, 79.
(8) Pausewang, V. G.; Schmitt, R.; Dehnicke K. *Z. Anorg. Allg. Chem.* **1974**, *408*, 1.
(9) Halasyamani, P.; Heier, K. R.; Stern, C. L.; Poeppelmeier, K. R. Unpublished results.

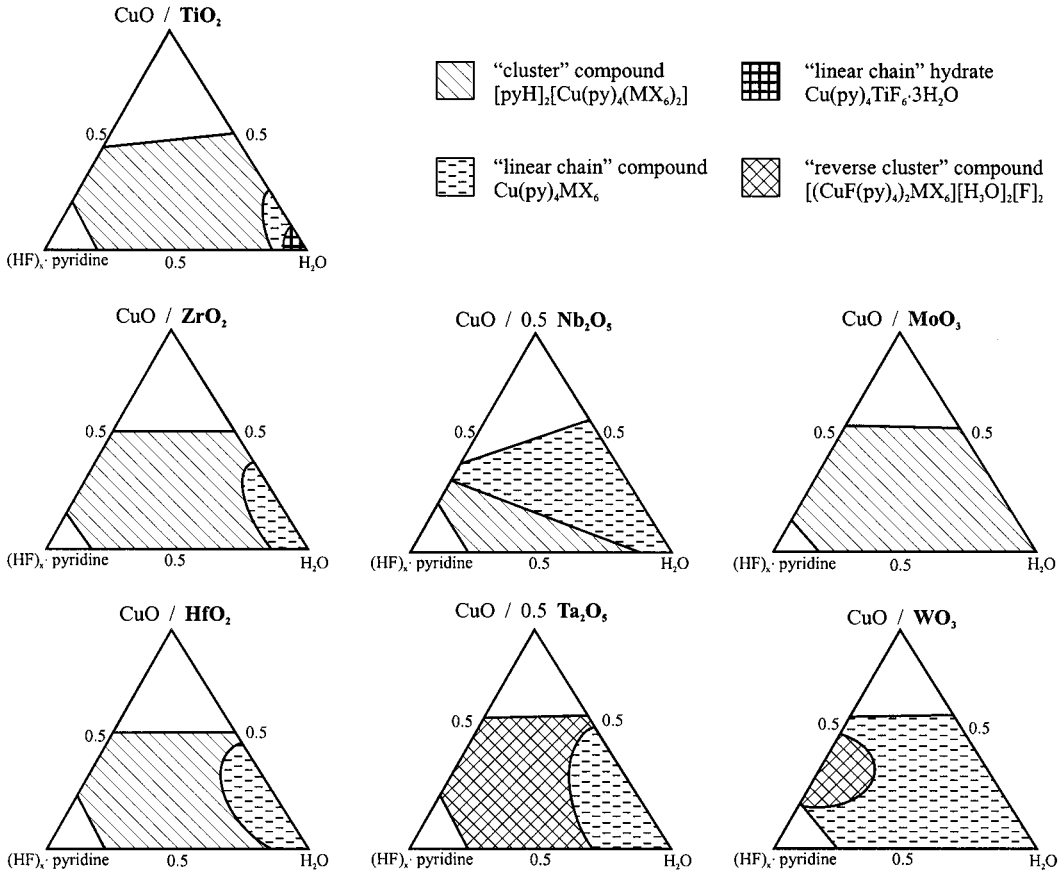

Figure 2. Composition space diagrams for the (CuO, M′O_x)/(HF)$_x$·pyridine/H_2O (M′O_x = TiO_2, ZrO_2, HfO_2, $^1/_2Nb_2O_5$, $^1/_2Ta_2O_5$, MoO_3, WO_3) systems.

further. At high (HF)$_x$·pyridine concentrations, all species remain in solution. $[M(py)_4]^{2+}$ and $[M'X_6]^{2-}$ are largely insoluble in pure pyridine at room temperature as a more polar medium is required to solvate the charged species. In the high (HF)$_x$·pyridine region of the composition space, the high H_3O^+ and F^- concentrations increase the polarity of the solution to such an extent that all species remain soluble. As a result, no solid products are available for analysis.

Anion Variation. Variation of the early transition metal oxide (M′O_x) in the system (CuO, M′O_x)/(HF)$_x$·pyridine/H_2O through the series TiO_2, ZrO_2, HfO_2, $^1/_2Nb_2O_5$, $^1/_2Ta_2O_5$, MoO_3, and WO_3 produces the $[TiF_6]^{2-}$, $[ZrF_6]^{2-}$, $[HfF_6]^{2-}$, $[NbOF_5]^{2-}$, $[TaOF_5]^{2-}$, $[MoO_2F_4]^{2-}$, and $[WO_2F_4]^{2-}$ anions, respectively. Subtle differences in these closely related anions cause significant variation in the crystallization fields in each system (Figure 2).

CuO TiO_2. The (CuO, TiO_2)/(HF)$_x$·pyridine/H_2O composition space consists of three crystallization fields. In the extreme H_2O corner of the composition space, a hydrated form of the linear chain compound is observed, $Cu(py)_4TiF_6·3H_2O$. The linear chain compound, $Cu(py)_4TiF_6$, forms at slightly less H_2O rich compositions where the pyH^+ concentration is still low. At the higher pyH^+ concentrations throughout the rest of the composition space, the cluster compound, $[pyH]_2[Cu(py)_4(TiF_6)_2]$, is the dominant phase.

CuO ZrO_2. The (CuO, ZrO_2)/(HF)$_x$·pyridine/H_2O composition space consists of two crystallization fields. The cluster compound, $[pyH]_2[Cu(py)_4(ZrF_6)_2]$, forms over the majority of the composition space. The linear chain compound, $Cu(py)_4ZrF_6$, forms only at low HF concentrations.

CuO HfO_2. The composition space for the (CuO, HfO_2)/(HF)$_x$·pyridine/H_2O system consists of two crystallization fields. The cluster compound, $[pyH]_2[Cu(py)_4(HfF_6)_2]$, forms over the majority of the composition space. The linear chain compound, $Cu(py)_4HfF_6$, forms only at low HF concentrations.

CuO $^1/_2Nb_2O_5$. Two crystallization fields exist in the (CuO, $^1/_2Nb_2O_5$)/(HF)$_x$·pyridine/H_2O composition space. At high (HF)$_x$·pyridine concentrations, where the probability of coordination by pyH^+ is high, the cluster compound, $[pyH]_2[Cu(py)_4(NbOF_5)_2]$, forms. The linear chain compound, $Cu(py)_4NbOF_5$, forms in lower HF concentrations where the relative pyH^+ concentration is low with respect to the $[Cu(py)_4]^{2+}$ concentration.

CuO $^1/_2Ta_2O_5$. The (CuO, $^1/_2Ta_2O_5$)/(HF)$_x$·pyridine/H_2O composition space consists of two crystallization fields. The reverse cluster compound, $[(CuF(py)_4)_2TaOF_5][H_3O]_2[F]_2$, forms over most of the composition space, except for the H_2O corner where the linear chain compound, $Cu(py)_4TaOF_5$, forms. The linear chain compound forms in the H_2O corner since the F^- and H_3O^+ concentrations are too low to form the hydrogen-bonding network displayed by the reverse cluster compound. The cluster compound does not form under these reaction conditions.

CuO MoO_3. The (CuO, MoO_3)/(HF)$_x$·pyridine/H_2O composition space consists of one crystallization field. The cluster compound, $[pyH]_2[Cu(py)_4(MoO_2F_4)_2]$, is the only phase over the entire composition space.

CuO WO_3. The (CuO, WO_3)/(HF)$_x$·pyridine/H_2O composition space consists of two crystallization fields. At low H_2O concentrations, the reverse cluster compound, $[(CuF(py)_4)_2WO_2F_4][H_3O]_2[F]_2$, forms. The linear chain compound, $Cu(py)_4WO_2F_4$, dominates the rest of the composition space. The reverse cluster compound requires high HF concentrations to form so that the

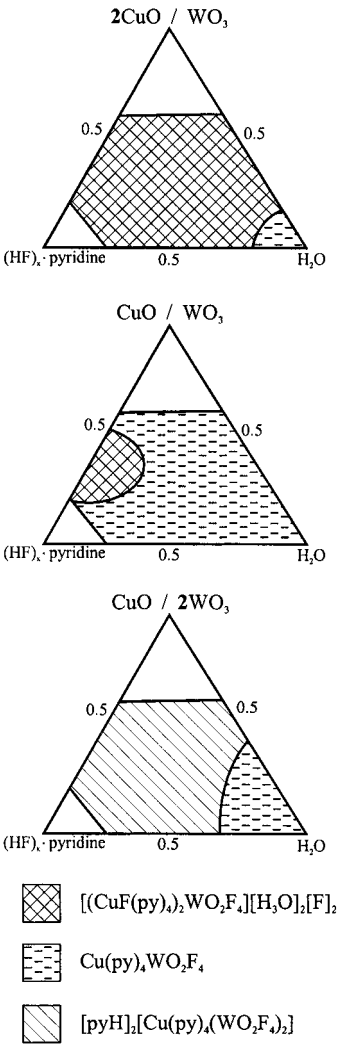

Figure 3. Composition space diagrams for the (CuO, $x$$WO_3$)/$(HF)_x$·pyridine/$H_2O$ (x = 0.5, 1, 2) systems.

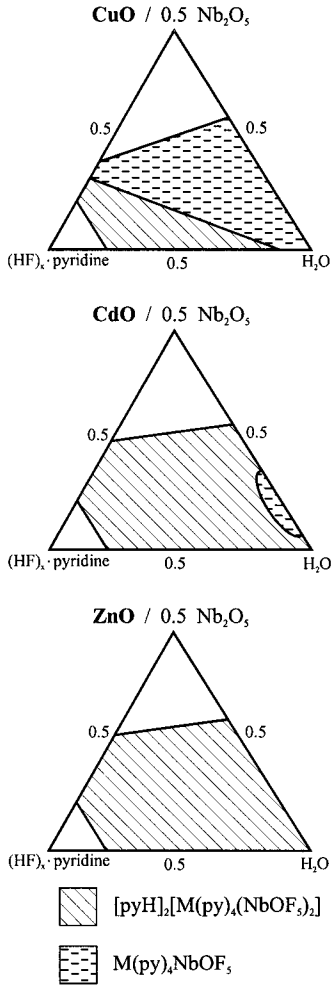

Figure 4. Composition space diagrams for the (MO, $^1/_2Nb_2O_5$)/$(HF)_x$·pyridine/H_2O (MO = CuO, CdO, ZnO) systems.

concentrations of F^- and H_3O^+ are large enough to form the hydrogen-bonding network present in the structure.

Each of these systems contains an $[MX_6]^{2-}$ anion. The anions $[ZrF_6]^{2-}$, $[NbOF_5]^{2-}$, $[MoO_2F_4]^{2-}$, and $[WO_2F_4]^{2-}$ are shown in Figure 5. If these anions are crystallographically ordered, that is, true bond lengths and not average bond lengths are known, bond valence calculations[10] can be employed to estimate the amount of negative charge on each O and F ligand (Table 2). The ligands with the most negative charge are the most nucleophilic and either coordinate to copper or become hydrogen bond acceptors for pyridinium (pyH^+). The structures and charge distribution on the ligands of the $[ZrF_6]^{2-}$, $[NbOF_5]^{2-}$, and $[MoO_2F_4]^{2-}$ anions have been previously discussed.[11] The charge distributions on $[MX_6]^{2-}$ anions formed in the (CuO, $M'O_x$)/$(HF)_x$·pyridine/H_2O ($M'O_x$ = ZrO_2, $^1/_2Nb_2O_5$, MoO_3, WO_3) systems help explain the differences in the crystallization fields of the cluster compounds, $[pyH]_2[Cu(py)_4(MX_6)_2]$ (MX_6 = ZrF_6^{2-}, $NbOF_5^{2-}$, $MoO_2F_4^{2-}$, and $WO_2F_4^{2-}$), and linear chain compounds, $Cu(py)_4MX_6$ (MX_6 = ZrF_6^{2-}, $NbOF_5^{2-}$, and $WO_2F_4^{2-}$).

To form a linear chain structure, two $[Cu(py)_4]^{2+}$ cations must coordinate to trans sites on an $[MX_6]^{2-}$ anion. The linear chain compound, $Cu(py)_4NbOF_5$, is formed readily because the most nucleophilic ligands on $[NbOF_5]^{2-}$ are trans to one another, making coordination of two $[Cu(py)_4]^{2+}$ cations favorable. However, linear chain formation is suppressed in the $CuO:ZrO_2$ system because the most nucleophilic ligands on $[ZrF_6]^{2-}$ are cis to one another. In this case, the differences in the negative charges on the ligands are small, as the anion is only slightly

Table 1. Crystallographic Data for $Cu(py)_4TaOF_5$ and $Cu(py)_4TiF_6{\cdot}3H_2O$

formula	$Cu(py)_4TaOF_5$	$Cu(py)_4TiF_6{\cdot}3H_2O$
empirical formula	$C_{20}H_{20}CuF_5N_4OTa$	$C_{20}H_{26}CuF_6N_4O_3Ti$
λ	0.710 69 Å	0.710 69 Å
fw	671.89	577.87
space group	*C*2/*c* (No. 15)	*C*2/*c* (No. 15)
a	10.541(3) Å	12.767(4) Å
b	13.547(6) Å	12.048(2) Å
c	16.04(1) Å	17.787(6) Å
β	97.73(5)°	109.9(1)°
V	2270(2) Å^3	2573(4)
Z	4	4
T	−120(1) °C	−120(1) °C
ρ_{calcd}	1.966 g cm^{-3}	1.492 g cm^{-3}
ρ_{obsd}[a]	1.939(4) g cm^{-3}	not measured[b]
μ	5.806 cm^{-1}	1.302 cm^{-1}
$R^c(F)$	0.022	0.060
$R_w{}^d(F)$	0.021	0.054

[a] Density measurements by flotation pycnometry at 25 °C. [b] Decomposes in pycnometry solvents. [c] $R = \sum||F_o| - |F_c||/\sum|F_o|$. [d] $R_w = [\sum w(|F_o| - |F_c|)^2/\sum w(F_o)^2]^{1/2}$.

(10) Brown, I. D.; Altermatt, D. *Acta Crystallogr., Sect B* **1985**, *41*, 244.
(11) Heier, K. R.; Norquist, A. J.; Wilson, C. G.; Stern, C. L.; Poeppelmeier, K. R. *Inorg. Chem.* **1998**, *37*, 76.

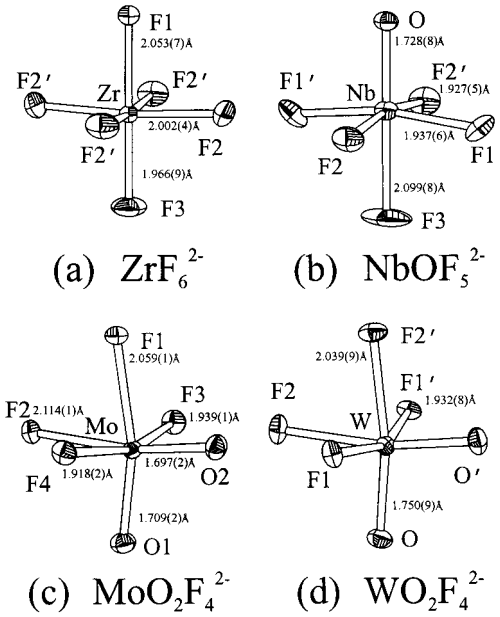

Figure 5. Thermal ellipsoid plots (50% probability) of the complex anions (a) ZrF_6^{2-},[11] (b) $NbOF_5^{2-}$,[1] (c) $MoO_2F_4^{2-}$,[11] and (d) $WO_2F_4^{2-}$,[12] with partial negative charge by each ligand.

Table 2. Bond Valence Sums[a,b] for ZrF_6^{2-}, $NbOF_5^{2-}$, and $MoO_2F_4^{2-}$

	R_i (Å)	S_i	ΣS_M	$(V - S_i)$
ZrF_6^{2-}				
			3.93	
Zr−F1	2.053(7)	0.57		0.43* [c]
Zr−F2	2.002(4)	0.66		0.34# [c]
Zr−F3	1.966(9)	0.72		0.28
$NbOF_5^{2-}$				
			5.08	
Nb═O	1.728(8)	1.64		0.36*
Nb−F1	1.937(6)	0.73		0.27
Nb−F2	1.927(5)	0.75		0.25
Nb−F3	2.099(8)	0.47		0.53#
$MoO_2F_4^{2-}$				
			5.86	
Mo═O1	1.709(2)	1.71		0.29
Mo═O2	1.697(2)	1.76		0.24
Mo−F1	2.059(1)	0.51		0.49*
Mo−F2	2.114(1)	0.44		0.56#
Mo−F3	1.939(1)	0.70		0.30
Mo−F4	1.918(2)	0.74		0.26
$WO_2F_4^{2-}$				
			5.84	
W═O	1.750(9)	1.57		0.43*
W−F1	1.932(8)	0.77		0.23
W−F2	2.039(9)	0.58		0.42#

[a] Bond valences calculated with the program Bond Valence Calculator v. 2.00, C. Hormillosa, S. Healy and T. Stephen, McMaster University (1993). [b] Valence sums calculated with the formula $S_i = \exp[(R_0 - R_i)/B]$ where S_i = bond valence of bond "*i*", R_0 = constant dependent on the bonded elements, R_i = bond length of bond "*i*", and $B = 0.370$. ΣS_M = bond valence sum for the metal. V = predicted valence for a site. R_0(Zr−F) = 1.846, R_0(Nb−O) = 1.911, R_0(Nb−F) = 1.822, R_0(Mo−O) = 1.907, R_0(Mo−F) = 1.808, R_0(W−O) = 1.917, and R_0(W−F) = 2.000. [c] (*) bound to Cu^{2+} (#) H-bond acceptor.

distorted. As a result, the linear chain compound is able to form in the CuO:ZrO_2 system at very low HF concentrations where the pyH^+ concentration is small, and coordination of $[Cu(py)_4]^{2+}$ is strongly favored over coordination of pyH^+. In the case of the $[MoO_2F_4]^{2-}$ anion, the linear chain compound does not form under any conditions because the ligands with the most negative charge are cis to one another. Unlike $[ZrF_6]^{2-}$, there is a large difference between the charges on cis and trans ligands, and $[MoO_2F_4]^{2-}$ is unable to coordinate another $[Cu(py)_4]^{2+}$ cation in a trans position to form the linear chains.

The $[WO_2F_4]^{2-}$ anion is unusual in that it has four highly nucleophilic ligands instead of the usual two (Table 2), allowing either cis or trans coordination. In both the $[WO_2F_4]^{2-}$ anion[12] and the analogous $[MoO_2F_4]^{2-}$ anion,[11] the M−F (M = Mo, W) bonds trans to the M═O bonds are long, leaving these fluorides with significant residual negative charge. However, the M═O bonds differ between the anions. In the $[MoO_2F_4]^{2-}$ anion, the Mo═O bonds are short, leaving little negative charge on the oxides. In the $[WO_2F_4]^{2-}$ anion, the W═O bonds are longer, leaving significant negative charge on the oxides. The most nucleophilic sites on the $[WO_2F_4]^{2-}$ anion are the two cis oxide ligands and the two fluorides trans to them. As a result, either cis or trans coordination is possible with $[WO_2F_4]^{2-}$. However, only trans coordination is observed in these systems, most likely in order to minimize cation−cation repulsion. In this respect, $[WO_2F_4]^{2-}$ is similar to $[NbOF_5]^{2-}$, as reflected in its large linear chain crystallization field.

Just as there are differences between the CuO:MoO_3 and CuO:WO_3 systems, there are also striking differences in the crystallization fields of the CuO:$^1/_2Nb_2O_5$ and CuO:$^1/_2Ta_2O_5$ systems (Figure 1). In this case, the differences can be explained through the relative concentrations of $[Cu(py)_4]^{2+}$ versus $[NbOF_5]^{2-}$ and $[TaOF_5]^{2-}$ in solution. In reactions throughout these two composition space diagrams, incomplete dissolution of Nb_2O_5 is rarely seen, while it is common for Ta_2O_5 even at low metal oxide mole fractions. This lowers the relative $[TaOF_5]^{2-}$ concentration to a level insufficient to form the two anion:one cation cluster compound.

The crystallization fields of the isovalent cluster, $[pyH]_2[Cu(py)_4(MF_6)_2]$, and linear chain, $Cu(py)_4MF_6$, compounds (M = Ti^{4+}, Zr^{4+}, and Hf^{4+}) and the hydrated linear chain species, $Cu(py)_4TiF_6 \cdot 3H_2O$, can be explained when the charge distributions and relative sizes of the $[TiF_6]^{2-}$, $[ZrF_6]^{2-}$, and $[HfF_6]^{2-}$ anions are considered. Six-coordinate Zr^{4+} and Hf^{4+} are nearly identical in size, 0.72 and 0.71 Å, respectively,[13] and are very similar chemically,[14] which is shown in their nearly identical composition space diagrams. The charge distribution of the $[TiF_6]^{2-}$ anion is believed to be very similar to that of $[ZrF_6]^{2-}$ and $[HfF_6]^{2-}$, and the crystallization fields of the linear chain and cluster compounds are similar. However, the CuO: TiO_2 system also displays a third compound, the hydrated linear chain, $Cu(py)_4TiF_6 \cdot 3H_2O$, in which the chains pack differently to allow water to hydrogen bond to the $[TiF_6]^{2-}$ anion. In $Cu(py)_4TiF_6 \cdot 3H_2O$, the linear chains stack in the *c*-direction on the $[Cu(py)_4]^{2+}$ cations, while in the normal linear chain compounds the chains stack on the $[MX_6]^{2-}$ anions (Figure 6). When the cations stack in the hydrated linear chain compound, channels are formed along the *c*-axis. Water occupies these channels, hydrogen bonding to the fluorides on the $[TiF_6]^{2-}$ anions. The existence of this compound is a consequence of the smaller $[TiF_6]^{2-}$ anion (ionic radius of 6-coordinate Ti^{4+} is 0.605 Å,[13]). The smaller dianion has a larger charge density and prefers to be more solvated than the other $[MX_6]^{2-}$ anions.

Metal Ratio Variation. The effects of changing relative metal concentrations are demonstrated in the CuO:WO_3 system. Three

(12) Chaminade, J. P.; Moutou, J. M.; Villeneuve, G.; Couzi, M.; Pouchard, M.; Hagenmuller, P. *J. Solid State Chem.* **1986**, *65*, 27.
(13) Shannon, R. D. *Acta Crystallogr., Sect A* **1976**, *32*, 751.
(14) Cotton, F. A.; Wilkinson, G. *Advanced Inorganic Chemistry, 5th ed.*; John Wiley & Sons: New York, 1988; p 777.

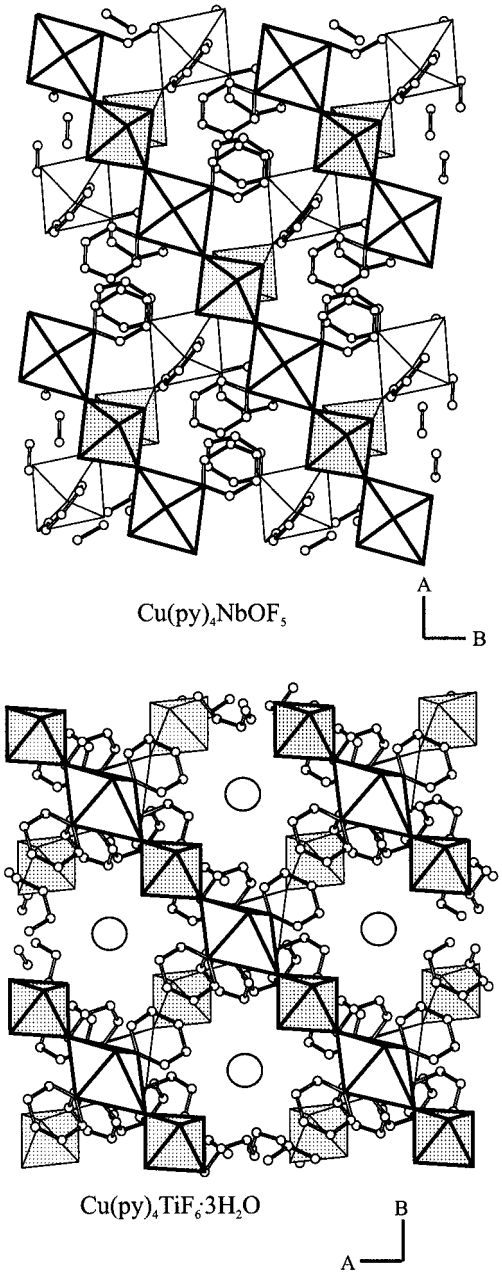

Figure 6. Packing diagrams of (a) $Cu(py)_4NbOF_5$ and (b) $Cu(py)_4TiF_6 \cdot 3H_2O$. Shaded octahedra represent $NbOF_5^{2-}$ and TiF_6^{2-}, and unshaded octahedra represent $Cu(py)_4^{2+}$. Circles (in b) represent H_2O.

composition space diagrams were constructed, with $CuO:WO_3$ mole ratios of 2:1, 1:1, and 1:2 (Figure 3).

$2CuO\ WO_3$. The $(2CuO, WO_3)/(HF)_x \cdot$pyridine/$H_2O$ composition space consists of two crystallization fields. At high H_2O concentrations, the linear chain compound, $Cu(py)_4WO_2F_4$, forms, but the reverse cluster, $[(CuF(py)_4)_2WO_2F_4][H_3O]_2[F]_2$, dominates the majority of the composition space.

$CuO\ 2WO_3$. The $(CuO, 2WO_3)/(HF)_x \cdot$pyridine/$H_2O$ composition space consists of two crystallization fields. At high H_2O concentrations the linear chain compound, $Cu(py)_4WO_2F_4$, forms. The cluster compound, $[pyH]_2[Cu(py)_4(WO_2F_4)_2]$, forms at higher HF concentrations.

As expected, the reverse cluster compound is the dominant product in the $2CuO:WO_3$ system owing to the higher $[Cu(py)_4]^{2+}$ concentration relative to the $[WO_2F_4]^{2-}$ concentration, although the linear chain compound still forms at high H_2O concentrations. When the $CuO:WO_3$ ratio is changed to 1:1, the reverse cluster compound is no longer favored and recedes to a much smaller region at low H_2O concentrations, while the linear chain crystallization field expands over the remainder of the composition space. The linear chain compound forms readily owing to the trans-directing nature of the $[WO_2F_4]^{2-}$ anion. The trend continues as the cluster compound, $[pyH]_2[Cu(py)_4(WO_2F_4)_2]$, is observed in the $CuO:2WO_3$ system. Throughout this composition space, except at very low $(HF)_x \cdot$pyridine concentration, the $[Cu(py)_4]^{2+}$ concentration is much lower than the pyH^+ concentration, leading to a much higher probability of the $[WO_2F_4]^{2-}$ anion being coordinated by a pyH^+ than by a second $[Cu(py)_4]^{2+}$. The only region where the linear chain compound dominates the crystalline products is at low $(HF)_x \cdot$ pyridine concentrations where little pyridinium is available for hydrogen bonding.

Cation Variation. Variation of the late transition metal oxide through the series CuO, CdO, and ZnO produces the $[Cu(py)_4]^{2+}$, $[Cd(py)_4]^{2+}$, and $[Zn(py)_4]^{2+}$ cations, respectively, and again causes significant differences in the composition space diagrams. The three composition space diagrams for the $(MO, {}^1/_2Nb_2O_5)/(HF)_x \cdot$pyridine/$H_2O$ (MO = CuO, CdO, and ZnO) systems are shown in Figure 4.

$CdO\ {}^1/_2Nb_2O_5$. The cluster compound, $[pyH]_2[Cd(py)_4(NbOF_5)_2]$, forms over the majority of the composition space. The linear chain compound, $Cd(py)_4NbOF_5$, forms at low HF concentrations.

$ZnO\ {}^1/_2Nb_2O_5$. The $(ZnO, {}^1/_2Nb_2O_5)/(HF)_x \cdot$pyridine/$H_2O$ composition space consists of only one crystallization field. The cluster compound, $[pyH]_2[Zn(py)_4(NbOF_5)_2]$, forms over the entire composition space. No linear chain compound is observed.

The cluster compounds, $[pyH]_2[M(py)_4(NbOF_5)_2]$ (M = Cu, Cd, and Zn) are isostructural, and the linear chain compounds, $M(py)_4NbOF_5$ (M = Cu and Cd), are structurally very similar. Despite these similarities, the composition space diagrams are quite different. The crystallization fields can be explained when the effects of cation reactivity with fluoride are considered. In the $CuO:{}^1/_2Nb_2O_5$ system, no CuF_2 is ever observed as a product. However, in the $CdO:{}^1/_2Nb_2O_5$ system, CdF_2 is seen in reactions at high $(HF)_x \cdot$pyridine concentrations. In the $ZnO:{}^1/_2Nb_2O_5$ system, ZnF_2 is observed throughout the composition space, even at low $(HF)_x \cdot$pyridine concentrations. ZnF_2 crystals are observed in the reaction pouches even before the samples are placed in the autoclave. Thermodynamic data ($\Delta_f H°$: CuF_2 = −542.7 kJ mol^{-1}, CdF_2 = −700.4 kJ mol^{-1}, and ZnF_2 = −764.4 kJ mol^{-1})[15] support these observations. The increased MF_2 formation in the Cd and Zn systems lowers the effective $[M(py)_4]^{2+}$ concentration, suppressing linear chain formation just as seen in the $CuO:2WO_3$ system described above. As a result, the crystallization field of the linear chain species is greatly reduced from the Cu system to the Cd system, and in the Zn system, the linear chain crystallization field disappears altogether.

Conclusion

Any systematic investigation of a hydrothermal reaction system can benefit from the use of composition space. Composition space diagrams have proven useful for planning hydrothermal reactions and rationalizing the results. For example, $Cu(py)_4TaOF_5$ was synthesized in good yield, without cocrystallization of other species, prior to completion of the composition space diagram. Plotting crystallization fields can

(15) Lide, D. R.; Frederikse, H. P. R., Eds; *CRC Handbook of Chemistry and Physics*, 74th Ed.; CRC Press: Boca Raton, 1993.

efficiently determine the conditions necessary to cleanly synthesize desired compounds. They also provide a convenient means of comparing and contrasting related reactions to help elucidate the factors governing phase stability.

Acknowledgment. The authors thank the following people, each of whom made an important contribution to the work presented here: Dr. P. Shiv Halasyamani, Michael J. Willis, Angel Duarte, Christopher G. Wilson, Catherine Lundin, Jennifer L. Brosius, Prof. Claude Mertzenich, and Katherine L. Eisele. The authors gratefully acknowledge support from the National Science Foundation, Solid State Chemistry (Award No. DMR-9727516), and made use of central facilities supported by the MRSEC program of the National Science Foundation (Grant DMR-9632472) at the Materials Research Center of Northwestern University.

Supporting Information Available: ORTEP (50% probability) plots for the two compounds $Cu(py)_4TaOF_5$ and $Cu(py)_4TiF_6 \cdot 3H_2O$, and composition space diagrams, including individual reaction points, for each system (13 pages). X-ray crystallographic files, in CIF format, for these two compounds are available on the Internet only. Access and ordering information is given on any current masthead page.

IC9807238